Colloids and Surfaces A: Physicochemical and Engineering Aspects 712 (2025) 136443

Contents lists available at ScienceDirect

Colloids and Surfaces A: Physicochemical and Engineering Aspects

journal homepage: www.elsevier.com/locate/colsurfa

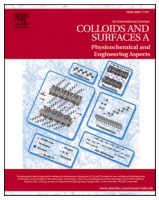

Role of dispersion nanostructure for bubble dissolution under pressure

Ivan Lesov [a], Hristo Alexandrov [a], Bozhidar Ivanov [b], Jessica Delavoipiere [c], Slavka Tcholakova [a,*]

[a] Department of Chemical and Pharmaceutical Engineering, Faculty of Chemistry and Pharmacy, Sofia University, Sofia, Bulgaria
[b] Institute of General and Inorganic Chemistry Bulgarian Academy of Sciences, Sofia, Bulgaria
[c] Saint Gobain Recherche, 39 quai Lucien Lefranc, Aubervilliers 93303, France

GRAPHICAL ABSTRACT

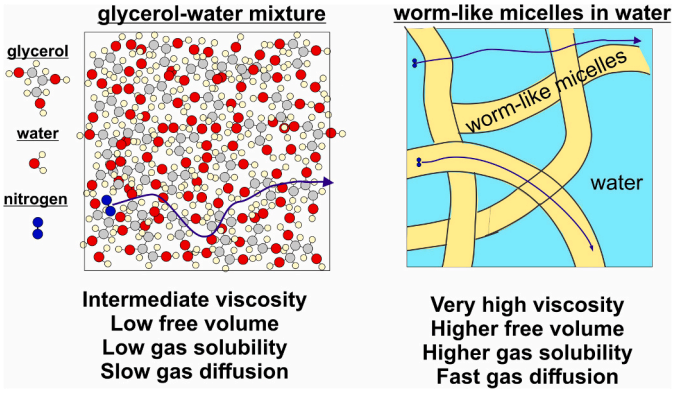

ARTICLE INFO

Keywords:
Nanoviscosity
Worm-like micelles
Diffusion coefficient
Gas solubility
Surface permeability

ABSTRACT

Understanding the factors that affect bubble dissolution under pressure is crucial for the pneumatic transport of dispersions. This study probes the kinetics of air dissolution, the air solubility at a given pressure, and the gas diffusion due to bubble dissolution to elucidate the molecular mechanisms of gas transport in liquid dispersions with varied structures and viscosities. We achieve our aims by using water-glycerol mixtures, silicone oils with different viscosities, surfactant solutions containing worm-like micelles and having different macroscopic viscosities, particle suspensions, and surfactant solutions capable of forming a condensed adsorption layer on the bubble surfaces at ambient conditions. The results show that the dissolution rate does not depend on the macroscopic viscosity for silicone oils and solutions containing worm-like micelles, indicating that gas diffusion occurs faster than the movement of big polymeric molecules and worm-like micelles. We could predict the experimentally determined diffusion coefficients by accounting for free volume in these media and using the equation for Knudsen diffusion. We show that one way to decrease the rate of bubble dissolution under pressure

Abbreviations: BS, Surfactant solution containing SLES + CAPB at 2:1 ratio; CAPB, Cocamidopropyl betaine; PDMS, Polydimethylsiloxane; SLES, Sodium laureth sulfate; SE, Stokes-Einstein equation.

* Correspondence to: Department of Chemical and Pharmaceutical Engineering, Faculty of Chemistry and Pharmacy, Sofia University, 1 James Bourchier Ave., Sofia 1164, Bulgaria.
E-mail address: SC@LCPE.UNI-SOFIA.BG (S. Tcholakova).

https://doi.org/10.1016/j.colsurfa.2025.136443
Received 13 December 2024; Received in revised form 2 February 2025; Accepted 16 February 2025
Available online 17 February 2025

is to add surfactants, which can decrease the permeability of the adsorption layer formed on the bubble surface by forming a condensed adsorption layer.

Nomenclature

a	hydrodynamic radius of the dissolved gas molecules
D	Diffusion coefficient, m^2/s
D_g	Diffusion coefficient of gas molecule in the silicone oil
Dg,a	Diffusion coefficient of gas molecule in air
C_0	Solubility of gas in a fluid medium, $g.m^{-3}$ bar^{-1}
$C_{0,N2}$, $C_{0,O2}$	gas solubility, denoting the bulk concentration of nitrogen and oxygen respectively
$C_{0N2\sigma}$, $C_{0O2\sigma}$	gas solubility, denoting the surface concentration of nitrogen and oxygen around the bubbles
C_{0P}	Solubility of gas in a fluid medium under pressure
C_1^0	gas solubility in pure water
C_1	gas solubility in electrolyte solution
C_2	concentration of electrolyte
k_{SCC}	solubility constant
k_B	Boltzmann constant, $J.K^{-1}$
n_{SE}	Stokes-Einstein number (dimensionless)
R	Radius of a bubble, μm
P	Pressure, bars
T	Temperature, K
α	Rate of dissolution, $μm^2/s$
γ	Parameter for gas distribution around a bubble, dimensionless
η	Viscosity, Pa.s
θ_g	Intermolecular porosity (dimensionless)
ρ_g	Mass density of gas, kg/m^3
φ,φ_{max}	Volume fraction and close-packing fraction of solid particles (dimensionless)

1. Introduction

The air bubbles dissolution under pressure is central to pneumatic transport of dispersions, used in cosmetics, foods and beverages, safety applications (e.g. fire extinguishing), and even 3-D printing of materials. The dissolution leads to local supersaturation with gas and might trigger subsequent nucleation or disproportionation via enhanced Ostwald ripening. Critical examples include processing structural materials such as concrete and polymer foams, where precise structural control is a must. Local fluctuations in size and volume fraction can lead to significant fluctuations in material properties and failure during settling and utilization.

Studies on gas solubility often employ isochoric saturation, a technique in which a specific volume is saturated with gas under pressure. The subsequent decrease in pressure over time is measured to evaluate the amount of dissolved gas [1,2]. Another approach involves gravimetric saturation at a constant pressure, where the mass of the dissolved gas is measured following a typically prolonged waiting period [1,2]. For the characterization of gas solubility, micellar solutions are to be considered non-isotropic. Micelles are proven to solubilize gas efficiently in their hydrophobic core, depending on their tail size and the nature of the dissolving gases [3–7]. It has been shown that the solubility of gases increases linearly with surfactant concentration above the critical micellar concentration for both anionic SDS and cationic CTAB [3]. The gas distribution coefficients between the SDS micelles and the surrounding water increased from 40 for oxygen to 350 for ethane [3]. The increase in carbon chain length of the gas from ethane to propane further increased the solubility in SDS and CTAB micelles [4]. The distribution coefficient of nitrogen between water and C_nTAB micelles was determined to increase with the surfactant chain length from 66 for DTAB to 70 for TTAB [6]. The high salt concentrations of up to 0.6 M NaCl in the aqueous phase did not affect the solubility of ethane in SDS micelles [7]. In these studies [3–7], the micelles were "classical" spherical micelles, which have a discrete nature compared to the worm-like micelles observed in some surfactant mixtures [8,9]. Such elongated micelles have the potential to enhance gas diffusion depending on their structure - a case that has been observed for Winsor I emulsions transitioning to Winsor III type [10]. However, as claimed, each gas's intermicellar solubility remains lower than its solubility in a typical hydrocarbon, as shown in [3].

Different techniques to study the gas transport in fluids were recently reviewed and classified in groups by Upreti and Mehrotra [11]. They include gravimetric and volumetric methods with multiple variations, as well as more sophisticated methods such as light or particle scattering [12,13], nuclear-magnetic resonance [14], membrane-based methods [15,16], computer modeling [17–19], and others [20–22]. Many of these techniques require sophisticated and expensive equipment and high specificity, limiting their use to several key substances. Therefore, their use could be hindered by non-isotropic solutions and emulsions.

To access both the gas solubility and the gas diffusion within homogeneous and heterogeneous dispersions, here we combine optical observation of single micrometric bubble dissolution under pressure [23–26] with independent measurement of the gas solubility via gravimetry [1,2]. This bubble dissolution technique was first developed by Epstein & Plesset in 1950 and demonstrated to work well for evaluating gas solubility in water [25–30] and oily drops in surfactant solutions [31,32] and ambient pressures. The gas diffusion in water for different gases was studied in [27] at temperatures between 10 and 60 °C at ambient pressure by measuring the bubble size decrease over time in the thermostated cell by using the method developed by Houghton et al. [26]. It was shown [27] that the diffusion coefficients of dissolved air can be estimated from those of oxygen and nitrogen at all temperatures. In a recent study of Cadogan et al. [33] the gas diffusivity was measured by Taylor dispersion method [34] at different temperatures and pressures, and it was shown that the results from Taylor dispersion method were 40 % lower as compared to the results obtained by the method of Wise & Houghton [27]. The effect of pressure up to 45 MPa was negligible on the measured diffusion coefficients [33]. The good agreement between experimental data obtained by Taylor dispersion method and the correlation based on the Stokes-Einstein equation was established in [33]. To our knowledge, the gas diffusivity of air in water-glycerol mixtures has not been tested, and it is unclear whether the Stokes-Einstein equation can be applied to these systems. In the current study, we applied the bubble diminishing technique to determine the gas dissolution kinetics in various complex media by applying different pressures during the dissolution stage.

It was shown in [35] that the oxygen mobility in cured poly(dimethylsiloxane) films is 5 orders of magnitude higher than that estimated by Stokes-Einstein when the macro-viscosity was used. The difference between micro-viscosity and macro-viscosity of polymer films explained the observed discrepancy. In [36], the molecular mobility in a series of silicone oils with different viscosities ranging between 1 and 2.5×10^6 mPa.s was determined by measuring the quenching rate constant of

pyrene fluorescence by phthalic anhydride. It was shown that the quenching rate constant is proportional to $\eta^{-0.4}$ for silicone oils with macro-viscosity, $\eta < 50$ mPa.s and the effect of macro-viscosity of silicone oils became even less pronounced for silicone oils with $\eta > 50$ mPa.s giving the dependence of quenching rate constant on $\eta^{-0.04}$ [36]. The estimated diffusion coefficients of phthalic anhydride in used silicone oils based on the measured quenching rate constants were found to vary between 1.4×10^{-9} m^2/s and 2.2×10^{-10} m^2/s, whereas the estimated viscosities based on Stokes-Einstein equation by using the measured macro-viscosities varied between 9.3×10^{-10} m^2/s and 3.7×10^{-16} m^2/s [36]. This considerable difference was explained by the difference between macro-viscosity and micro-viscosity [36], where the macro-viscosity arises from the movement of the complete PDMS molecule. In contrast, the micro-viscosity depends on the motion of a part of the molecule (segmental or side group movement) [36]. The introduction of silyl or siloxane structures in ionic liquids also increased solute diffusivity in these systems, but the effect is much smaller than in silicone oils [37]. The deviation of solute diffusivity in ionic liquids from the Stokes-Einstein equation was explained by three factors: flexibility, interaction energy, and free volume [37]. In [38], it was shown that the ratio between experimentally measured diffusion coefficient and predicted by the Stokes-Einstein equation depends on the nature of the solute molecules and solvent molecules. For neutral solutes, the empirical equation for predicting the deviation from Stokes-Einstein prediction is proposed based on the ratios of the solute-to-solvent van der Waals volumes. A similar approach is used in [14] to describe the experimental data for diffusion coefficients measured at different pressures. It is unknown whether the approach developed for ionic liquids can be used for other systems and for what systems we can expect large deviations from Stokes-Einstein prediction and for which we can apply it.

Therefore, the primary aim of the current study is to use the simple bubble diminishing technique to investigate gas dissolution at room temperature at different pressures in various types of systems: water, water-glycerol mixtures, silicone oils, surfactant solutions with different types of micelles having very different macroscopic viscosities, saponin solution which ensures the formation of dense adsorption layer on the diminishing bubble [39,40] and silica suspension.

2. Materials

We prepared the solutions using deionized water purified via the Elix 3 module (Millipore). We used sodium chloride to adjust the electrolyte concentration and analytical grade glycerol for its aqueous solutions (both from Teokom, Bulgaria). We used the following surfactants: Escin - a product of Sigma (Cat. No. 50531) and purity > 95 %. We mixed 10 wt % sodium laureth sulfate, SLES (Steol CS270, Stepan, 70 % activity) and cocamidopropyl betaine, CAPB (Tegobetain F50, Evonik, 40 % active) in 2:1 wt:wt ratio. Their mixtures are abbreviated as BS in the text from this point on. Then, the calculated amount of sodium chloride was added as a powder to the solutions and homogenized for a couple of hours before use.

We purchased polydimethylsiloxane or PDMS with various viscosities, AK10, 100, 1000, 2000, and 30000 cSt from Wacker, and silica nanoparticles Ludox TM50 from Sigma Aldrich.

We used N_2 (Sol Bulgaria) and ambient air with 20–50 % relative humidity for the dissolution experiments. All experiments were performed at 25 ± 3°C.

3. Methods

3.1. Gas solubility

10–25 g of fluid was placed in a sapphire tube (26 mm inner diameter, 2.5 mm thickness, 100 mm height; Saint Gobain Crystals) and sealed with Teflon-coated alumina plates. A manual ball valve on top sealed the cell under pressure. The cell's mass was measured (± 0.01 g accuracy; Precisa 165 BJ Series, BJ 2200 C). To measure the gas solubility, we designed a procedure that resembles gravimetric solubility measurements used for hydrogen sorption [41]. We measured the cell's mass with the fluid before and after compression with nitrogen between 10 and 50 bars, depending on the expected gas solubility. Higher pressures were used for lower gas solubility to achieve higher masses. The mass under pressure was measured immediately after compression, and the fluid within the cell was stirred continuously during the saturation with a magnetic stirrer. The mass of the fluid increased gradually and reached a constant value after equilibrium saturation. The final change in the mass under pressure was recorded and divided by the saturation pressure and the initial sample mass to yield the gas solubility, C_0, in g.m^{-3}.bar^{-1}. We removed the excess pressure and measured the mass of the supersaturated fluid again. Then, we stirred the fluid to remove the excess gas, which nucleated into bubbles. We recorded the mass for the third time when all the bubbles coalesced with air. In the end, we averaged the three measurements.

We measured the solubility in surfactant solutions from the foam volume generated from supersaturation, decompression, and mixing for 20–30 seconds. The difference in the solution height before decompression and the foam maximum height after decompression and stirring was measured to estimate the air volume.

3.2. High-pressure optical observation cell

To study the dissolution of bubbles under pressure, we built a custom observation cell, like the one designed by Nishiyama in 2017 [42], but with a gas cylinder pressurization [43], see Fig. 1. We attached an uncoated sapphire with a 25 mm diameter and 3 mm thickness (WG30530, Thorlabs) to a stainless-steel mount via Norland optical adhesive 68TH. A 2 mm observation window with 1 mm internal height was left for optical observations in transmitted light (Nikon Labophot 2) via × 5 LD objective (Nikon E Plan). Manual ball valves (BKR up to 350 bars, Hansa Flex) were attached on both sides of the cell to allow sample injection, cell cleaning, compression, and decompression. We set the pressure in the outer tubing to the desired value via a pressure regulator (HD250, Hornung), and pressure was applied by opening the electromagnetic solenoid valves (1/4, AC 220 v, NPT) with 1.5 mm orifices that allow up to 300 bars pressure.

We recorded the bubble dissolution via a high-speed camera (Chronos 1.4, Kron Technologies). The high-speed camera allowed for 17500 frames to be recorded at 1240 × 1080 resolution and different frame rates (typically between 1000 and 100 fps), allowing for a recording between 17.5 and 175 seconds. We also used a regular microscope camera (Levenhuk M200) for simultaneous observation of slower dissolution that allowed unrestricted duration of the observation at 25 fps.

We prepared dispersions with a typical volume of 100 mL trapped and mixed them manually to trap a few bubbles. Then, we injected 20 mL of the fluid in the cell to rinse it. Another 20 mL was injected via syringe until a bubble settled in the observation window. Then, the bubble was left for at least 30 s to cream to the sapphire wall, and hydrostatic pressure was equilibrated. Afterward, we initiated the high-speed camera and compressed the fluid. We injected new solutions for each experiment and measured 3–5 bubbles for each system. We processed data for bubbles with a radius under pressure between 20 and 150 μm. We cleaned the cell after each dispersion using repeated flow injection of hot water, isopropanol, and ethanol (96 %). We used a cleaning solution of Decon 90 to soak the cell for several hours/days after using polymers. Finally, we dried the cell via continuous air pumping.

3.3. Dissolution rate evaluation and diffusion coefficient determination

We processed the video by isochronous slicing into 100 images using

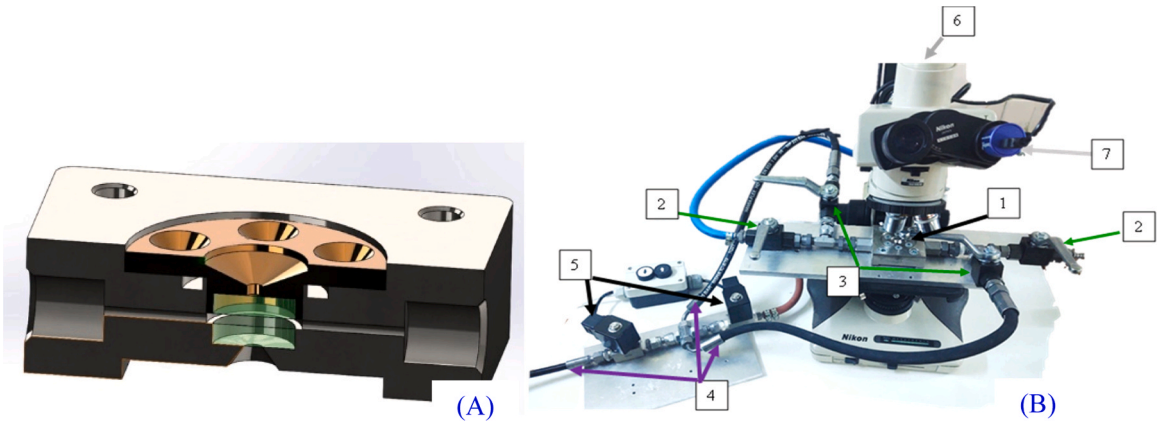

Fig. 1. Cell for optical observation of bubbles dissolution via under pressure. **(A)** A stainless-steel optical observation cell with pressure-resistant sapphire windows. **(B)** The pressure setup: The observation cell (1) is filled with bubbles-containing liquid by opening the ball valves (2). After filling the cell, valves (2) are closed, and ball valves (3) are opened towards the atmosphere to allow hydrostatic pressure equilibration. Then, the valve 5-in is opened to allow pressure simultaneously at both sides of the observation cell while the high-speed camera is used for recording the dissolution process. Pressure is applied via a gas cylinder with a pressure regulator (HD250, Hornung).

VideoProc Converter. Then, we used the images to estimate the projected area of the bubbles for each image using Fiji software (ImageJ). Next, we calculated the bubble radius vs time.

We processed the experimental results using three different theoretical procedures with different levels of complexity:

3.3.1. *Steady-state approximation*

The experimental data presented in the main text are obtained from the determined slope of bubble size decrease in the range $R/R_0 < 0.8$ and $R/R_0 > 0.5$, where R is the bubble's radius at time t, and R_0 is the initial radius of the bubble. The upper limit of 0.8 is chosen based on considerations in [28]. To minimize errors from data processing, data

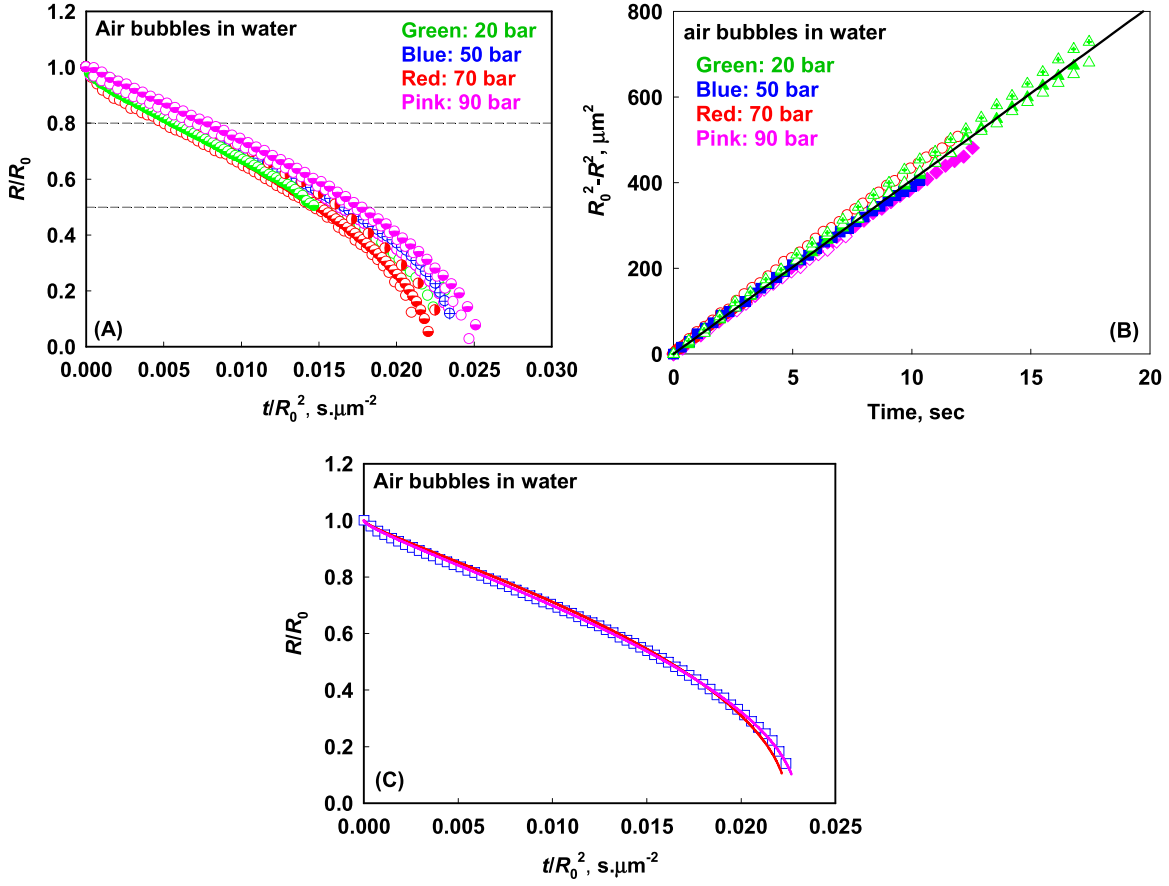

Fig. 2. (A) The evolution of scaled bubble radius R/R_0 as a function of scaled time t/R_0^2 for bubbles placed in water and observed at different pressures. The dashed lines indicate the region that is used to plot the data in (B) Bubble area as a function of time for air bubbles dissolved in water at different pressures. The points are experimental data obtained at different pressures, whereas the curves are calculated following Eq. (1) with $s_1 = 40.6$ μm^2/s; (C) The best description of experimental data for a single bubble in water at 20 bars by accounting for non-steady state distribution of air around the bubble with $s_2 = 38.2$ μm^2/s (red curve) and by presence of oxygen and nitrogen in the bubble with $s_{3,N2} = 34.1$ μm^2/s for nitrogen, $s_{3,O2} = 69.5$ μm^2/s for oxygen and $D_{N2}/D_{O2} = 1$ (pink curve).

for bubbles smaller in radius than 10 μm was measured but not used in the fitting procedures as error increased exponentially beyond this point at the magnification used. Thus, we discarded the data for $R/R_0 < 0.5$ for bubbles in water at higher pressures (Fig. 2). The experimental data followed a linear dependence when (R_0^2-R^2) was plotted as a function of t *with* a slope s_1:

$$R_0^2 - R^2 = s_1 t \tag{1}$$

According to the steady-state analysis given by Epstein & Plesset [25], the determined slope, s_1, is proportional to the diffusion coefficient. However, because the studied bubbles are much lighter than the surrounding liquid, they float up close to the upper side of the cell wall, which restricts gas diffusion. Liebermann introduced an empirical correction of 0.693 in [44] that varied up to 0.852 in [28]. Wise and Houghton [27] present a value of 0.686, which is in excellent agreement with our results:

$$\alpha_1 = \frac{s_1}{2k_1} \tag{2}$$

Where α_1 is the dissolution rate, and k_1 is the correction coefficient accounting for the solid wall above the bubble, equal to 0.69. From the rate of dissolution, we calculate the diffusion coefficient via [25]:

$$D_{EXP} = \alpha_1 \frac{\rho_g}{C_0 - C_i} \tag{3}$$

Where C_i is the initial gas concentration dissolved in the media, C_0 is the dissolved gas concentration in the media for a saturated solution at a given temperature and pressure, and ρ_g is the mass density of gas at a given pressure - a textbook value that is known for various gases and gas mixtures [45]. The value of C_i is neglected compared to the value of C_0 because the experiments are performed at least 20 bars, which means that even if the saturation solubility is reached at ambient pressure, the value of C_i is at least 20 times lower compared to C_0.

As noted above, the initial curve integration for $R/R_0 > 0.8$ effectively increases the dissolution coefficient s_1 by around 10 %, while k_1 decreases it by ≈ 45 %, meaning that the two corrections lead to a typical value of $\alpha_1 \approx 1.30$ when compared to a steady state integration over the whole curve.

3.3.2. *Accounting for non-steady state distribution of gas around diminishing bubble*

Epstein and Plesset [25] used steady-state approximation to derive eq. [1]. However, a non-stationary contribution is present during the initial stages of dissolution around the shrinking bubble [25]. To account for this effect, we solved numerically the equation accounting for non-stationary distribution, which is given in Ref. [25]:

$$\frac{dy}{dx} = -\frac{x}{y} - \gamma \tag{4}$$

Where γ is determined from the known values of C_0 and ρ_g for each system:

$$\gamma = \sqrt{\frac{2(C_0 - C_i)}{\pi \rho_g}} \tag{5}$$

From the best fit of experimental data plotted as R/R_0 vs. t/R_0^2 and numerically determined dependence of $y(x)$ at a given value of γ we determined the value of α_2 considering that:

$$y = \frac{R}{R_0}; x = \sqrt{\frac{s_2 t}{R_0^2}} \tag{6}$$

The values of α_2 and D_{EXP2} from determined values of s_2 are calculated by using Eqs. (2) and (3) above. Usually, the calculated values of α_2 are ≈ 30 % smaller than those of α_1 calculated from steady-state approximation.

3.3.3. *Accounting for the presence of two gases in the diminishing bubble*

The air is a mixture of nitrogen and oxygen. Oxygen has higher solubility in the aqueous solutions than nitrogen and a slightly higher diffusion coefficient. That is why, in the initial stages, oxygen dissolves faster in the surrounding media than nitrogen. The equations that describe the evolution of a bubble containing multiple molecules are derived in [29] to be:

$$D_{O_2} C_{O_2 S} \left(\frac{1}{R} + \frac{1}{\sqrt{\pi D_{O_2} t}} \right)^2 = D_{N_2} C_{N_2 S} \left(\frac{1}{R} + \frac{1}{\sqrt{\pi D_{N_2} t}} \right)^2 \tag{7}$$

$$\frac{C_{O_2 \sigma}}{C_{O_2 S}} + \frac{C_{N_2 \sigma}}{C_{N_2 S}} = 1 \tag{8}$$

$$P \frac{dR}{dt} = -kTD_{N_2} C_{N_2 \sigma} \left(\frac{1}{R} + \frac{1}{\sqrt{\pi D_{N_2} t}} \right) - kTD_{O_2} C_{O_2 \sigma} \left(\frac{1}{R} + \frac{1}{\sqrt{\pi D_{O_2} t}} \right) \tag{9}$$

C_{O2S} and C_{N2S} are the saturation concentrations of O_2 and N_2 at pressure P. Those are the values known from the literature, $C_{O2\sigma}$ and $C_{N2\sigma}$ are the concentrations of O_2 and N_2 at the boundary of the bubble on the solution side. Note that for one component system $C_{O2S} = C_{O2\sigma}$. R is the bubble radius, k is the Boltzmann constant, T is the temperature, D_{N2} and D_{O2} are the diffusion coefficients of N_2 and O_2.

3.4. *Viscosity measurements*

We measured the viscosity of solutions and dispersions via rotational rheometer Bohlin Gemini with cone and plate geometry 40 mm diameter and 4° cone angle. We used the viscosity interval between 0.01 and 300 s^{-1} for micellar solutions and fit the experimental data with the Carreau model to extract the zero-shear viscosity. The other dispersions we used were Newtonian liquids, and their viscosity was independent of the shear rate.

4. Experimental results and discussion

4.1. *Solutions viscosity*

The experimental results for measured viscosities of the media used for bubble dissolution are shown in Fig. S1 in the Supporting Information. The chosen media have very different rheological responses: (1) Silicone oils, water-glycerol mixtures and silica suspensions have nearly Newtonian behavior with viscosities ranging between 0.89 mPa.s up to 30×10^5 mPa.s; (2) BS solutions with low electrolyte concentrations also show nearly Newtonian behavior, see red circles in Fig. S1C; (3) BS solutions with high electrolyte concentrations have shear thinning behavior, see Fig. S1A and S1B. For these solutions, the viscosity decreases with the increase of shear rate, and it is not clear in advance which viscosity the gas molecules "feel" during their diffusion through such media.

4.2. *Gas solubility in studied systems*

Table 1 summarizes the experimental data for gas solubility in studied dispersions. Our method yields reasonable results compared to various literature sources, apart from glycerol and 70 % glycerol-water mixture. As presented in the methods section, our gravimetric method has a resolution of ± 0.01 g, equivalent to ± 8 $g.m^{-3}.bar^{-1}$ for 50 bars pressure and 25 mL solution. To improve the measurement accuracy, we modified the procedure to measure the volume of the dissolved gas with a resolution of ± 3 $g.m^{-3}.bar^{-1}$: we measured 20 mL of 1 wt% escin (which had a negligible effect on gas solubility in water) in 70 wt% glycerol solution. We saturated the solution at 20 bars under continuous stirring overnight. Then, we decompressed the samples and stirred them

Table 1
Gravimetric air solubility at 25 °C in different dispersions. The symbol "÷" represents the ranges of data scattering across the different literature sources, given in the brackets. The error bars in the experiments represent the data scattering for a resolution of ± 8 g.m^{-3}.bar^{-1}.

System		$C_{0\,P}$, g.m^{-3}.bar^{-1}	
		Experiment	Reference data
Water-glycerol mixtures	Water	19 ± 5	18 (15÷20) [1, 46][i] 42 (26÷45) [46, 47][ii]
	70 % glycerol	18 ± 8	6.0 (5.2÷6.7) [2, 48,49][iii]
	> 99 % glycerol	13 ± 4	5.7 (2.3÷9.0) [2, 48,49][iv]
Silicone oils	AK10	270 ± 50	160 [50][v]
	AK100	250 ± 50	260 [50][vi]
	AK1000	250 ± 50	169 ± 6 [51][vii] 100 ± 9 [15][viii] 232 ± 13 [15][ix] 285 [52][x]
Surfactant solution	wt% BS	22.5 ± 3	20[xi]
	wt% BS + 220 mM NaCl	23 ± 9	44[xii]
Silica dispersion	50 wt% Ludox	16.6 ± 1.3 total 13.2 in water 3.4 sorption at particle surface	16.5 [53][xiii] 13.2 3.3 [53][xiv]

The number in the parenthesis shows the reference from which the data are taken. [i]N_2 in water at 25 °C; [ii]O_2 in water at 25 °C; [iii]N_2 in 67–70 wt% aqueous solution of glycerol at 15–25 °C; [iv] N_2 in glycerol at 15 °C; [v]N_2 in AK100 at 25 °C; [vi]O_2 in AK100 at 25 °C; [vii]O_2 in PDMS with a viscosity of 26 Pa.s at 30 °C; [viii]N_2 in PDMS film cross-linked at 35 °C; [ix]O_2 in PDMS film cross-linked at 35 °C; [x]Air in silicone fluids KF96 at 25 °C; [xi] Calculated solubility of N_2 in BS+NaCl solution at 25 °C without accounting for Laplace pressure in the micelles; [xii]Calculated solubility of O_2 in BS+NaCl solution at 25 °C without accounting for Laplace pressure in the micelles; [xiii]Calculated, assuming 35 % air sorption at particles interface, using data for activated carbon at 20 °C at 5 bars.

at low speed to trigger bubble nucleation. As a result, foam grew from the dissolved supersaturated gas. We measured the final foam volume and estimated the amount of dissolved gas, corresponding to 13 ± 3 g.m^{-3}.bar^{-1} for 70 wt% glycerol. This value is in line with our gravimetric measurements (18 ± 8 g.m^{-3}.bar^{-1}) and showed higher gas solubility in the used glycerol and glycerol-water mixtures than those presented in the literature. There are two possible explanations for the observed discrepancy between our data and those reported in the literature for glycerol solutions: (1) insufficient accuracy of our experimental method or (2) insufficient saturation time in the methods used in the literature. Currently, we cannot conclude which is the primary reason for the observed discrepancy. On the other hand, the discrepancy is much lower for all other systems in which the gas solubility is higher. Therefore, we can make unambiguous conclusions about the gas diffusivity in the complex mixtures with gas solubility higher than 10 g.m^{-3}.bar^{-1}.

The solubility in silicone oils is much higher than in aqueous solutions, and the obtained results are in the order of magnitude of values reported in the literature. An increase in solubility within the experimental error is measured in surfactant solutions, which agrees with results reported in the literature [3–7].

To calculate the maximal solubility of oxygen and nitrogen in the SLES-CAPB (BS) solutions at different salt concentrations, we used the expressions known from the literature for the effect of salt concentration on the solubility of O_2 and N_2 in the water. We used the following expression [2,46,47]:

$$\log \frac{C_1^0}{C_1} = k_{SCC} C_2 \tag{10}$$

Where C_1^0 is the gas solubility in pure water, C_1 is the gas solubility in the electrolyte solution, C_2 is the molar concentration of electrolyte, and k_{SCC} is 0.141 L/mol [47] for O_2 and 0.129 L/mol [2,46] for N_2. To account for solubility inside the surfactant micelles, we used the molar ratios of 1.23 × 10^{-3} [2] for N_2 and 2.1946 × 10^{-3} [47] of O_2 dissolved in $C_{12}H_{26}$. To account for the Laplace pressure of the micelle interior, we used the model proposed in [3], which shows that the actual solubility of gas molecules in micelles interior will be ≈ 50 % smaller as compared to their solubility in bulk alkanes. The estimated values of C_{0P} for 10 wt% BS+ 220 mM NaCl are shown in Table 1. Note that CAPB in BS contains 1.12 mol NaCl for each mole of CAPB [9]. The calculated value for the solubility of N_2 is very close to that measured by our experimental method.

4.3. Kinetics of air bubble dissolution in water

We measured the dissolution of at least two bubbles in pure water at four different pressures of 20, 50, 70, and 90 bars. The experimental results are analyzed using the three approaches described in section 2.2 to determine the diffusion coefficients. The experimental data and their description by the used approaches are shown in Fig. 2, whereas the determined diffusion coefficients and the used values for gas solubility are shown in Table 2. One sees that the description of the experimental results accounting for the presence of two gases in the bubble is better as compared to the case when only one gas is accounted for, see red and pink curve in Fig. 2 C, because the initial slope is higher as compared to the final slope showing that the oxygen is dissolved first.

The determined values for diffusion coefficients in water do not depend on the applied pressure in the frame of our experimental accuracy. The value of the diffusion coefficient determined from the linear regression is slightly higher than that determined from the description of the results using Eq. (4). This is because the value of γ in Eq. (4) becomes negligible when the bubble radius becomes smaller than 20 μm, which is close to the minimal bubble radius we processed. Therefore, neglecting γ in Eq. (4) and using Eq. (1) for the description of experimental results, we overestimated the value of s_1 by 15 %.

The determined values of the diffusion coefficients of nitrogen and oxygen molecules in water agree with the results reported in the literature. The value of 2.0 × 10^{-9} m^2/s is reported for diffusion of N_2 in water at pressures between 12 and 45 MPa in [33]. A slightly higher value of 2.6 × 10^{-9} m^2/s at 20 °C is reported in [27], but in that case the experimental data for bubble dissolution are described by Eq. (1) by using the initial slope of the curve, which further overestimated the diffusion coefficient value. The value of 1.75 × 10^{-9} m^2/s was used in [28] to describe the air bubble dissolution in water. We use Eq. (1) to determine the diffusion coefficients for air molecules in different media.

The next stage was to compare the obtained diffusion coefficients with the predicted on the base of the Stokes-Einstein equation [33]:

$$D_{SE} = \frac{k_B T}{n_{SE} \pi \eta a} \tag{11}$$

Where k_B is Boltzmann constant, T is temperature, η is the solvent viscosity, a is the hydrodynamic radius of the solute, n_{SE} is the

Table 2
Determined diffusion coefficients of gas molecules from best fit of experimental data for bubble size decrease at different pressures using three approaches described in Section 2.

	Gas	ρ_g/C_0	γ	s, μm^2.s^{-1}	D_{EXP}, m^2/s
Steady-state	Air	61.5	0	40.6 ± 1.6	(1.8 ± 0.1)× 10^{-9}
Non-steady state	Air		0.102	36.7 ± 2.2	(1.6 ± 0.1)× 10^{-9}
Non-steady state Two components	N_2	62.6	0.101	33.4 ± 2.2	(1.5 ± 0.1)× 10^{-9}
	O_2	30.7	0.144	61.5 ± 4.5	(1.4 ± 0.1)× 10^{-9}

Stokes−Einstein number. For non-slip boundary conditions, the value of $n_{SE} = 6$ for spherical particles, whereas for slip boundary conditions $n_{SE} = 4$. In [33], the value of $n_{SE} = 4$ is used to calculate the diffusion coefficient of nitrogen in water, but the overall view is that a value of 4 should be used for self-diffusion coefficients, whereas a value of 6 for diffusion of solute in solvents with different molecular structure [54,55]. Here, we use $n_{SE} = 4$ to calculate the diffusion coefficients by Eq. (11) to avoid underestimating the diffusion coefficient as suggested in [55]. The value of a is 190 pm for nitrogen molecules, as in [33]. The calculated value of D_{SE} is 1.9×10^{-9} m^2/s, which is close to one estimated from the best fit of experimental data by Eq. (1).

4.4. Kinetics of air bubble dissolution in water-glycerol mixtures

We performed the experiments to determine the bubble dissolution in water-glycerol mixtures at 50 bars. The comparison between diffusion coefficients determined from the bubble diminishing experiment and Eq. (11) are shown in Table 3. The values determined from bubble diminishing experiments for water and water-glycerol mixtures seem close to ones estimated from SE equation. The slight increase in D_{EXP}/D_{SE} with the increase of glycerol content is very close to the frame of our experimental accuracy, considering the uncertainties in the measured gas solubility in glycerol solutions. One possible reason for the observed increase in D_{EXP}/D_{SE} could be the higher free volume around one glycerol molecule, when compared to the free volume around one water molecule, which increases the rate of gas transport in the glycerol-water mixture.

4.5. Kinetics of air bubble dissolution in surfactant solutions

Next, we focused on heterogeneous structures, starting with micellar solutions. We investigated the effect of the transition from elongated to worm-like micelles. We prepared SLES-CAPB (BS) solutions in a 2:1 wt ratio and varied the electrolyte concentration to obtain elongated micelles, and worm-like structures [9]; see Fig. S1 in SI. As shown in Ref. [9], elongated micelles are formed at low electrolyte concentration in 10 wt% BS which transform into worm-like micelles at higher electrolyte concentrations. Clear indication for this transition is the change in the rheological properties of the micellar solutions. The solutions containing spherical or slightly elongated micelles exhibit Newtonian behavior with viscosity of the order of that of pure water, whereas the solutions containing worm-like micelles exhibit very high zero-shear viscosity at low shear rates, with a linear decrease above a certain critical shear rate. From the studied solutions, 10 wt% BS and 1 wt% BS+ 300 mM NaCl exhibit Newtonian behavior and, hence, contain slightly elongated micelles. In contrast, the solutions of 5 wt% BS+ 300 mM NaCl; 10 wt% BS + 100 mM NaCl; 10 wt% BS+ 200 mM NaCl; and 10 wt% BS+ 1 wt% tetradecanoic acid exhibit a very well pronounced plateau region at low shear rates and a linear decrease at high shear rate, viz. they contain worm-like micelles.

We determined the bubble dissolution rates, α, for micellar solutions with different concentrations of surfactant and salt concentrations. The experimental results are presented in Table 4. One sees that the determined diffusion coefficients for all studied systems are very close to each other and very close to diffusion coefficients determined for water solutions alone. In these media, the increase of apparent viscosity of the media does not change the diffusion coefficient of gas molecules. This unexpected result means the gas molecules travel between the worm-like micelles without filling them. Further discussion on this point is given in Section 4.7 below.

Table 3
Diffusion coefficients of gas molecules, estimated from best fit of experimental data for bubble size decrease vs predicted values from Stokes-Einstein equation.

	η, mPa.s	ρ_g/C_0	D_{EXP}, m^2/s	D_{SE}, m^2/s	D_{EXP}/D_{SE}
Water	0.89	61.5	$(1.8 \pm 0.1)\times 10^{-9}$	1.9×10^{-9}	0.9 ± 0.3
70.0 % glycerol	17.7	65 ± 29	$(1.5 \pm 0.8)\times 10^{-10}$	9.7×10^{-11}	1.6 ± 0.8
99.5 % glycerol	775	90 ± 28	$(4.6 \pm 1.4)\times 10^{-12}$	2.2×10^{-12}	2.1 ± 0.6

4.6. Kinetics of air bubble dissolution in silica suspensions

The next stage was to determine the rate of bubble dissolution in the silica suspensions, which had Newtonian behavior, as seen in Fig. S1. The obtained results from this series of experiments are summarized in Table 5. One sees that the diffusion coefficient is also very close to one determined for water solutions, and it decreases 2 times upon increase of the silica concentration from 0 to 50 wt%.

4.7. Kinetics of air bubble dissolution in silicone oils

The experimental results for bubble dissolution in used silicone oils are summarized in Table 6. One sees that the dissolution rate is much faster in silicone oils than in aqueous solutions, but the estimated diffusion coefficients in different silicone oils are very close to those measured for water solution. It should be mentioned that these diffusion coefficients are in excellent agreement with the results reported in the literature. In [15], the diffusion coefficient of 3.4×10^{-9} m^2/s was reported for oxygen and nitrogen in PDMS film at 35 °C. In [56], the diffusion coefficient of air molecules in 500 cSt silicone oil is measured and it was found that the diffusion coefficient at 303 K is $\approx 5.1 \times 10^{-9}$ m^2/s.

4.8. Comparison between different diffusion coefficients

The determined diffusion coefficients in water and silicone oils agree well with the experimental results reported in the literature. The comparison between measured and theoretically predicted diffusion coefficients based on the Stokes-Einstein equation for the slip case shows good agreement between measured and theoretically calculated results for water and water-glycerol mixtures and a deviation for other more viscous solutions and oils. The higher the viscosity, the larger the deviation between measured and estimated diffusion coefficients.

Such differences are already discussed in the literature for diffusion coefficients of different gas molecules in hydrocarbons [57], polyatomic liquids [58], ionic liquids [37–39,59], etc. Ref. [60] used molecular dynamics simulations to demonstrate that the diffusion coefficient of small solutes is significantly higher than predicted by the Stokes-Einstein equation when calculated using the mean square displacement of moving molecules. However, it aligns closely with the prediction of the SE equation when estimated using the time correlation function of the force acting on fixed solutes. This discrepancy arises because the solvent structure relaxes more quickly through solute motion, while the motion of solvent molecules is necessary for fixed or larger solutes. Additionally, Ref. [58] explicitly stated that the SE equation fails when the solute molecule's size is much smaller than that of the solvent molecule. It was shown in [58] that the ratio between the actual diffusion coefficient and one determined via SE depends on the ratio of the excluded volume of a solute molecule with the volume per solvent molecule expressed as $n\sigma_{12}^3$ where n is the number density of the solvent and σ_{12} is the sum of the radii of the solvent and solute molecules. The deviation from SE becomes negligible when $n\sigma_{12}^3$ approaches unity. These authors [58] proposed a rigid particle model to account for deviations from SE, but as they stated, the proposed model is inapplicable to predicting the diffusion through H-bonding liquids and n-tetradecane. We applied this approach for the diffusion of air molecules in silicone oils, but the values of $n\sigma_{12}^3$ are very similar for different oils, whereas D_{EXP}/D_{SE} varies significantly, showing that this is not the main effect. A similar conclusion is drawn if we plotted D_{EXP}/D_{SE} as a function

Table 4
The experimental data for viscosity at plateau region, the rate of bubble dissolution, s_1, the ratio between gas density and its estimated solubility ρ_g/C_0, the measured diffusion coefficient, and SE diffusion coefficients for aqueous surfactant solutions. BS stands for the mixture of SLES:CAPB in 2:1 wt ratio.

Surfactant concentration	η, mPa.s	ρ_g/C_0	α, μm^2.s^{-1}	D_{EXP}, m^2/s	D_{SE}, m^2/s	D_{EXP}/D_{SE}
wt% BS + 300 mM NaCl	4.2	55.3	26.5 ± 2.5	(1.5 ± 0.1)× 10^{-9}	4.1 × 10^{-10}	3.7 ± 0.3
wt% BS+ 300 mM NaCl	1750	52.1	39.1 ± 2.6	(2.0 ± 0.1)× 10^{-9}	9.8 × 10^{-13}	2000 ± 400
wt% BS	22.0	51.9	23.3 ± 1.8	(0.9 ± 0.1)× 10^{-9}	8.6 × 10^{-11}	10.1 ± 1.2
wt% BS + 1wt% tetra-decanoic acid	350	45.0	25.9 ± 2.1	(1.2 ± 0.1)× 10^{-9}	4.9 × 10^{-12}	245 ± 20
wt% BS + 100 mM NaCl	3300	46.1	32.6 ± 1.9	(1.5 ± 0.1)× 10^{-9}	5.2 × 10^{-13}	2900 ± 200
wt% BS + 200 mM NaCl	28000	47.3	30.6 ± 2.6	(1.4 ± 0.1)× 10^{-9}	6.1 × 10^{-14}	23000 ± 2000
wt% Escin	1.0	58.3	14.3 ± 0.4	(0.8 ± 0.1)× 10^{-9}	1.7 × 10^{-9}	0.5 ± 0.05

Table 5
The experimental data for measured viscosity at plateau region, the rate of bubble dissolution, α, gas solubility, C_{OP}, estimated diffusion coefficient from measured values of α C_{OP} and calculated diffusion coefficient from Stoks-Einstein equation for aqueous Ludox suspensions.

Ludox concentration	η, mPa.s	α, μm^2.s^{-1}	$C_{0\,P}$, g.m^{-3}.bar^{-1}	D_{EXP}, m^2/s	D_{SE}, m^2/s	D_{EXP}/D_{SE}
wt%	2.3	20.9 ± 2.7	20.8 ± 3	(1.2 ± 0.3)× 10^{-9}	7.5 × 10^{-10}	1.6 ± 0.4
wt%	5.1	19.8 ± 1.9	21.7 ± 3	(1.1 ± 0.3)× 10^{-9}	3.3 × 10^{-10}	3.2 ± 0.8
wt%	32.9	12.6 ± 0.7	22.6 ± 3	(0.7 ± 0.2)× 10^{-9}	5.2 × 10^{-11}	12.5 ± 2.0

Table 6
The experimental data for measured viscosity at plateau region, the rate of bubble dissolution, α, the gas solubility, C_{OP}, estimated diffusion coefficient from measured values of α and C_{OP} and calculated diffusion coefficient from Stoks-Einstein equation for PDMS oils.

PDMS oil	η, mPa.s	α, μm^2.s^{-1}	$C_{0\,P}$, g.m^{-3}.bar^{-1}	D_{EXP}, m^2/s	D_{SE}, m^2/s	D_{EXP}/D_{SE}
AK10	10	420 ± 130	270 ± 50	(1.8 ± 0.6)× 10^{-9}	1.7 × 10^{-10}	10.6 ± 3.7
AK100	100	540 ± 60	250 ± 50	(2.4 ± 0.5)× 10^{-9}	1.7 × 10^{-11}	136 ± 29
AK1000	1000	500 ± 100	250 ± 50	(2.2 ± 0.6)× 10^{-9}	1.7 × 10^{-12}	1270 ± 360
AK30000	30000	460 ± 70	250 ± 50	(2.0 ± 0.5)× 10^{-9}	5.7 × 10^{-14}	34600 ± 8240

of the volume ratio between solute and solvent molecules as proposed in [38].

The results reported in Table 6 show that the diffusion coefficients are practically independent of the macroscopic viscosity, showing that the diffusion of gas molecules is decoupled from the diffusion of the silicone molecules, as suggested in [60]. Therefore, the gas molecules diffuse around the silicone molecules as in Knudsen diffusion, see Fig. 3C. Note that a similar explanation is given in [61] for the diffusion of hydrogen molecules through modified rubbers. Assuming that we can use the equation that has been derived for gas diffusion through the undisturbed soil [62], which is given by the expression:

$$D_g = 0.45\theta_g^3 D_{g,a} \quad (12)$$

Where D_g is the diffusion coefficient through the silicone oil, $D_{g,a}$ is the diffusivity in free air, θ_g is the porosity. Calculations after Bondi [63] show that $\theta_g = 0.30 \pm 0.03$ (see Supplementary Information). Molecular simulations in cured PDMS show a value of 0.19 that increases to 0.43 with decreasing the volume of the solute molecules [64]. Using $D_g = 2.2 \times 10^{-9}$ m^2/s and $D_{g,a} = 1.1 \times 10^{-7}$ m^2/s., we obtain θ_g around 0.343, which practically coincides with averaged data for 6500 homopolymers used in membrane separation techniques for gases [65].

The next stage is to explain the results for silica suspensions. In that case, the solid particles affect the diffusion of the gas molecules through the water phase, as discussed for the self-diffusion coefficient in colloidal dispersions [66–68]. Assuming that the cell model that was shown to describe well the experimental data for the self-diffusion of colloidal silica can also apply to the diffusion of gas molecules inside the water, the following expression can be used [68]:

$$\frac{D_g}{D_{g.w}} = \left(1 - \frac{\varphi}{\varphi_{max}}\right)^2 \quad (13)$$

Where φ is the volume fraction of suspended particles, φ_{max} is the volume fraction of the particles at close-packing ≈ 0.64, $D_{g,w}$ is the gas diffusion coefficient in the bulk water. The predicted values of D_g via Eq. (13) for Ludox suspensions are 1.2 × 10^{-9} m^2/s (25 wt% Ludox with φ = 12.8 %); 0.8 × 10^{-9} m^2/s (37.5 wt% Ludox with φ = 21 %) and 0.5 × 10^{-9} m^2/s (50 wt% Ludox with φ = 30.7 %) are in excellent agreement with the experimental data shown in Table 5 showing sterically limited diffusion of the gas, which resembles the self-diffusion of colloidal particles [68].

The experimental results for micellar solutions are more challenging to predict with high precision because the gas molecules can diffuse through the aqueous media and the interior of the worm-like micelles. The diffusion coefficients of oxygen through water and hexadecane were found to be close to each other at 22 °C (2.1 ×10^{-9} m^2/s in water and 2.5 ×10^{-9} m^2/s in hexadecane) in [69]. Therefore, as a first approximation, we can expect that the diffusion coefficient of worm-like micelles will be very close to one measured in water and hexadecane, which is ≈ 2 × 10^{-9} m^2/s. The data presented in Table 4 shows that the determined values for different surfactant solutions are close to that one, which shows that the gas molecules diffuse through both media, and that is why there is no significant difference between them. A higher accuracy of the gas solubility measurements might allow better discrimination of the structural effects currently within the experimental error.

The experimental results for water-glycerol mixtures are in relatively good agreement with predicted diffusion coefficients from the Stokes-Einstein equation, see Table 3. This suggests that the free volume around the water and glycerol molecules, through which the gas molecules can diffuse, is much smaller than that of the silicone oils. We used the approach developed in [63,70] to calculate the free accessible gas volume. We estimated the difference between the molecular volume and the van der Waals volume that we compared with the nitrogen molecule with a value of 28 A^3 [63,70]. The calculated volumes are shown in Table S1. The free volume per water molecule is 13 A^3, much smaller than the van der Waals volume of nitrogen. Thus, the water can be considered as continuous media for the diffusion of nitrogen, and the

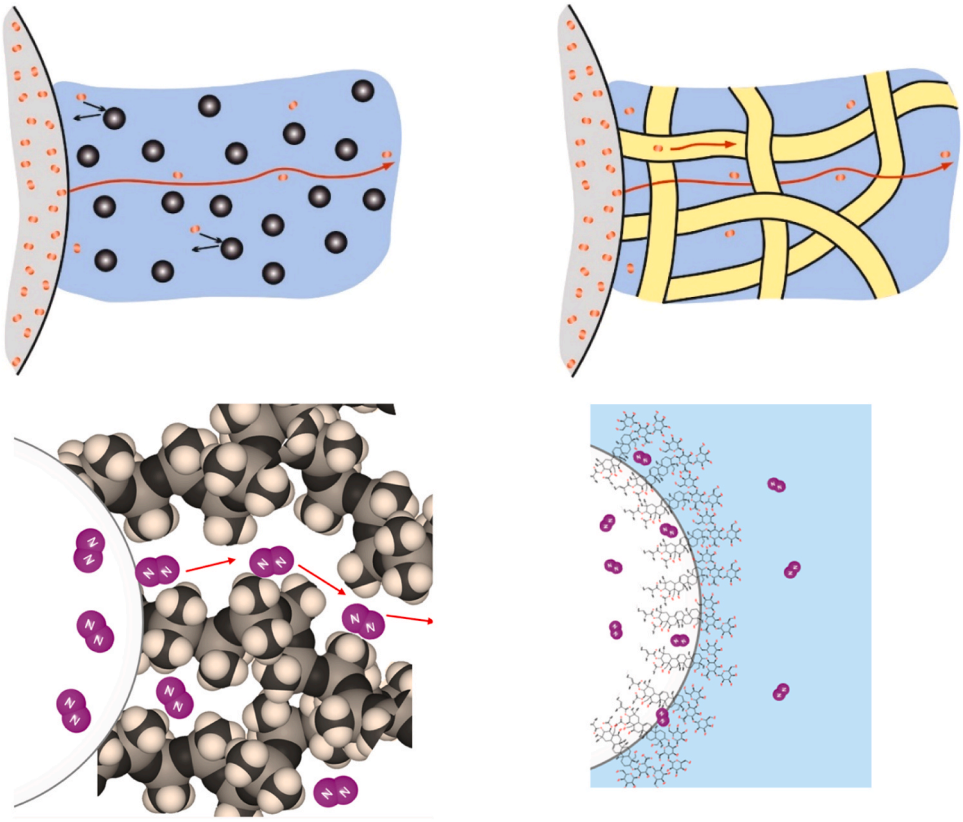

Fig. 3. Schematic representation of nitrogen diffusion through (A) silica suspensions; (B) solution of worm-like micelles; (C) silicone oils; (D) escin solution.

diffusion coefficient of nitrogen can be predicted using SE. The free volume around the glycerol is ≈ 38.52 A^3, which is comparable to a nitrogen molecule's van der Waals radius. Therefore, for this glycerol solution, the measured diffusion coefficient is 2-fold higher than the one predicted by SE.

Finally, we will discuss the lower diffusion coefficient measured for Escin solutions as compared to one predicted by SE. In fact, this is the only diffusion coefficient with a lower value than one predicted by SE. This lower value can only be explained via a condensed surfactant layer at the bubble interface that reduces the gas migration rate from the bubble interior into the solution. A similar effect was shown to be operative for the rate of Ostwald ripening in escin-stabilized foams [39].

5. Conclusions

The study reveals that the micro- and nanostructures within dispersions significantly influence the gas diffusion rates. The water-glycerol solutions that are typically used in cosmetics and foam applications conform to traditional models, whereas worm-like micellar solutions and polymer melts (such as PDMS) exhibit accelerated dissolution rates due to nanoviscosity effects. These findings suggest that we need new methods to evaluate the nanoviscosity and the media structural effects whenever mass flows are to be considered.

Future research should focus on the detailed molecular mechanisms driving these observations and their implications for industrial applications involving pneumatic transport and material processing. Manufacturers can achieve better control over product quality and performance by understanding and manipulating the factors that affect bubble dissolution and gas diffusion.

Funding

This study is financed by Saint Gobain Research and by the European Union-Next Generation EU, through the National Recovery and Resilience Plan of the Republic of Bulgaria, project № BG-RRP-2.004–0008-C01.

CRediT authorship contribution statement

Lesov Ivan: Writing – review & editing, Writing – original draft, Visualization, Methodology, Investigation, Formal analysis, Conceptualization. **Alexandrov Hristo:** Investigation. **Ivanov Bozhidar:** Investigation. **Tcholakova Slavka:** Writing – review & editing, Supervision, Methodology, Formal analysis, Conceptualization. **Delavoipiere Jessica:** Funding acquisition, Conceptualization.

Declaration of Competing Interest

The authors declare that they have no known competing financial interests or personal relationships that could have appeared to influence the work reported in this paper.

Appendix A. Supporting information

Supplementary data associated with this article can be found in the online version at doi:10.1016/j.colsurfa.2025.136443.

Data availability

Data will be made available on request.

References

[1] R. Battino, T.R. Rettich, T. Tominaga, The solubility of nitrogen and air in liquids, J. Phys. Chem. Ref. Data. 13 (1984) 563–600, https://doi.org/10.1063/1.555713.

[2] A. Schumpe, G. Quicker, W.-D. Deckwer, Gas solubilities in microbial culture media, in: Reaction Engineering. Adv Biochem Eng Biotechnol, 24, Springer, Berlin/Heidelberg, 1982, pp. 1–38, https://doi.org/10.1007/3-540-11699-0_9.

[3] I.B. Matheson, A. King, Solubility of gases in micellar solutions, J. Colloid Interface Sci. 66 (1978) 464–469, https://doi.org/10.1016/0021-9797(78)90066-8.

[4] S. Roy, A. Mehra, D. Bhowmick, Prediction of solubility of nonpolar gases in micellar solutions of ionic surfactants, J. Colloid Interface Sci. 196 (1997) 53–61, https://doi.org/10.1006/jcis.1997.5181.

[5] B. Meng, H.S. Ashbaugh, Effect of hydrostatic pressure on gas solubilization in micelles, Langmuir 31 (2015) 3318–3325, https://doi.org/10.1021/la503646z.

[6] L.C.A. Garzon, A.F. Suarez, C.M. Romero, Solubility of argon and nitrogen in aqueous solutions of tetradecyltrimethylammonium bromide from 283.15 to 298.15 K and 101,325 Pa partial pressure of gas, J. Therm. Anal. Calorim. 128 (2017) 475–479, https://doi.org/10.1007/s10973-016-5888-6.

[7] J.C. Hoskins, A.D. King, The effect of sodium chloride on the solubility of ethane in micellar solutions of sodium dodecyl sulfate, J. Colloid Interface Sci. 82 (1981) 264–267, https://doi.org/10.1016/0021-9797(81)90151-X.

[8] M. Pleines, W. Kunz, T. Zemb, D. Benczédi, W. Fieber, Molecular factors governing the viscosity peak of giant micelles in the presence of salt and fragrances, J. Colloid Interface Sci. 537 (2019) 682–693, https://doi.org/10.1016/j.jcis.2018.11.072.

[9] Z. Mitrinova, H. Alexandrov, N. Denkov, S. Tcholakova, Effect of counter-ion on rheological properties of mixed surfactant solutions, Colloids Surf. A 643 (2022) 128746, https://doi.org/10.1016/j.colsurfa.2022.128746.

[10] M. Petzold, N. Paul, L. Hohl, L. Böhm, M. Kraume, Gas/liquid mass transfer phenomena in micellar multiphase systems, Chem. Eng. Process. - Process. Intensif. 171 (2022) 108547, https://doi.org/10.1016/j.cep.2021.108547.

[11] S.R. Upreti, A.K. Mehrotra, Experimental determination of gas diffusivity in liquids - a review, Can. J. Chem. Eng. 99 (2021) 1239–1267, https://doi.org/10.1002/cjce.23984.

[12] A. Leipertz, A.P. Fröba, Diffusion measurements in fluids by dynamic light scattering. Diffusion in Condensed Matter, Springer-Verlag, Berlin/Heidelberg, 2005, pp. 579–618, https://doi.org/10.1007/3-540-30970-5_15.

[13] D. Kivelson, P.A. Madden, Light scattering studies of molecular liquids, Annu. Rev. Phys. Chem. 31 (1980) 523–558, https://doi.org/10.1146/annurev.pc.31.100180.002515.

[14] Y. Kimura, Y. Kida, Y. Matsushita, Y. Yasaka, M. Ueno, K. Takahashi, Universality of viscosity dependence of translational diffusion coefficients of carbon monoxide, diphenylacetylene, and diphenylcyclopropenone in ionic liquids under various conditions, J. Phys. Chem. B. 119 (2015) 8096–8103, https://doi.org/10.1021/acs.jpcb.5b02898.

[15] T.C. Merkel, V.I. Bondar, K. Nagai, B.D. Freeman, I. Pinnau, Gas sorption, diffusion, and permeation in poly(dimethylsiloxane), J. Polym. Sci. Part B Polym. Phys. 38 (2000) 415–434, https://doi.org/10.1002/(SICI)1099-0488(20000201)38:3< 415::AID-POLB8> 3.0.CO;2-Z.

[16] J. Park, H. Ha, H.W. Yoon, J. Noh, H.B. Park, D.R. Paul, C.J. Ellison, B.D. Freeman, Gas sorption and diffusion in poly(dimethylsiloxane) (PDMS)/graphene oxide (GO) nanocomposite membranes, Polym. (Guildf.) 212 (2021) 123185, https://doi.org/10.1016/j.polymer.2020.123185.

[17] Y. Tamai, H. Tanaka, K. Nakanishi, Molecular simulation of permeation of small penetrants through membranes. 1. Diffusion coefficients, Macromol 27 (1994) 4498–4508, https://doi.org/10.1021/ma00094a011.

[18] D. Hofmann, L. Fritz, J. Ulbrich, D. Paul, Molecular simulation of small molecule diffusion and solution in dense amorphous polysiloxanes and polyimides, Comput. Theor. Polym. Sci. 10 (2000) 419–436, https://doi.org/10.1016/S1089-3156(00)00007-6.

[19] H. Shirota, E.W. Castner, Why are viscosities lower for ionic liquids with -$CH_2Si(CH_3)_3$ vs -$CH_2C(CH_3)_3$ substitutions on the imidazolium cations? J. Phys. Chem. B. 109 (2005) 21576–21585, https://doi.org/10.1021/jp053930j.

[20] L. Ferguson, P. Scovazzo, Solubility, diffusivity, and permeability of gases in phosphonium-based room temperature ionic liquids: data and correlations, Ind. Eng. Chem. Res. 46 (2007) 1369–1374, https://doi.org/10.1021/ie0610905.

[21] Y. Gong, H. Wang, Y. Chen, X. Hu, A.-R. Ibrahim, A.-R. Tanyi, Y. Hong, Y. Su, J. Li, A high-pressure quartz spring method for measuring solubility and diffusivity of CO_2 in ionic liquids, Ind. Eng. Chem. Res. 52 (2013) 3926–3932, https://doi.org/10.1021/ie400267h.

[22] J. Zhang, A.R. Teixeira, H. Zhang, K.F. Jensen, Flow toolkit for measuring gas diffusivity in liquids, Anal. Chem. 91 (2019) 4004–4009, https://doi.org/10.1021/acs.analchem.8b05396.

[23] P. Peñas-López, M.A. Parrales, J. Rodríguez-Rodríguez, D. van der Meer, The history effect in bubble growth and dissolution. Part 1. Theory, J. Fluid Mech. 800 (2016) 180–212, https://doi.org/10.1017/jfm.2016.401.

[24] P. Peñas-López, Á. Moreno Soto, M.A. Parrales, D. van der Meer, D. Lohse, J. Rodríguez-Rodríguez, The history effect on bubble growth and dissolution. Part 2. Experiments and simulations of a spherical bubble attached to a horizontal flat plate, J. Fluid Mech. 820 (2017) 479–510, https://doi.org/10.1017/jfm.2017.221.

[25] P.S. Epstein, M.S. Plesset, On the stability of gas bubbles in liquid-gas solutions, J. Chem. Phys. 18 (1950) 1505–1509, https://doi.org/10.1063/1.1747520.

[26] G. Houghton, P.D. Ritchie, J.A. Thomson, The rate of solution of small stationary bubbles and the diffusion coefficients of gases in liquids, Chem. Eng. Sci. 17 (1962) 221–227, https://doi.org/10.1016/0009-2509(62)85001-5.

[27] D.L. Wise, G. Houghton, The diffusion coefficients of ten slightly soluble gases in water at l0-60°C, Chem. Eng. Sci. 21 (1966) 999–1010, https://doi.org/10.1016/0009-2509(66)85096-0.

[28] S. Kentish, J. Lee, M. Davidson, M. Ashokkumar, The dissolution of a stationary spherical bubble beneath a flat plate, Chem. Eng. Sci. 61 (2006) 7697, https://doi.org/10.1016/j.ces.2006.08.071.

[29] C.A. Ward, A.S. Tucker, Thermodynamic theory of diffusion−controlled bubble growth or dissolution and experimental examination of the predictions, J. Appl. Phys. 46 (1975) 233, https://doi.org/10.1063/1.321327.

[30] C. Yung, K.J. De Witt, J. Brockwell, J. McQuillen, A. Chai, A numerical study of parameters affecting gas bubble dissolution, J. Colloid Interface Sci. 127 (1989) 442, https://doi.org/10.1016/0021-9797(89)90049-0.

[31] K.L. Chong, Y. Li, C.S. Ng, R. Verzicco, D. Lohse, Convection-dominated dissolution for single and multiple immersed sessile droplets, J. Fluid Mech. 892 (2020) A21, https://doi.org/10.1017/jfm.2020.175.

[32] P.D. Todorov, P.A. Kralchevsky, N.D. Denkov, G. Broze, A. Mehreteab, Kinetics of solubilization of n-decane and benzene by micellar solutions of sodium dodecyl sulfate, J. Colloid Interface Sci. 245 (2002) 371–382, https://doi.org/10.1006/jcis.2001.8031.

[33] S.P. Cadogan, G.C. Maitland, J.P.M. Trusler, Diffusion coefficients of CO_2 and N_2 in water at temperatures between 298.15 K and 423.15 K at pressures up to 45 MPa, J. Chem. Eng. Data 59 (2014) 519–525. ⟨https://pubs.acs.org/doi/10.1021/je401008s⟩.

[34] G. Taylor, Dispersion of soluble matter in solvent flowing slowly through a tube, Proc. R. Soc. Lond., Ser. A. 219 (1953) 186–203, https://doi.org/10.1098/rspa.1953.0139.

[35] D.Y. Chu, J.K. Thomas, J. Kuczynski, Photophysical studies of molecular mobility in polymer films. Oxygen mobility in polymer films monitored by quenching of the triplet-triplet absorption of bromopyrene, Macromol 21 (7) (1988) 2094–2100, https://doi.org/10.1021/ma00185a037.

[36] D.Y. Chu, J.K. Thomas, Photophysical studies of molecular mobility in polymer films and bulk polymers. 2. Quenching of pyrene fluorescence by phthalic anhydride in bulk poly(dimethylsiloxanes), J. Phys. Chem. 93 (1989) 6250–6257, https://doi.org/10.1021/j100353a056.

[37] T. Endo, S. Nemugaki, Y. Matsushita, Y. Sakai, H. Ozaki, Y. Hiejima, Y. Kimura, K. Takahashi, Fast solute diffusivity in ionic liquids with silyl or siloxane groups studied by the transient grating method, Chem. Phys. 472 (2016) 128–134, https://doi.org/10.1016/j.chemphys.2016.03.016.

[38] A. Kaintz, G. Baker, A. Benesi, M. Maroncelli, Solute diffusion in ionic liquids, NMR measurements and comparisons to conventional solvents, J. Phys. Chem. B. 117 (2013) 11697–11708, https://doi.org/10.1021/jp405393d.

[39] S. Tcholakova, F. Mustan, N. Pagureva, K. Golemanov, N.D. Denkov, E.G. Pelan, S. D. Stoyanov, Role of surface properties for the kinetics of bubble Ostwald ripening in saponin-stabilized foams, Colloids Surf. A Physicochem. Eng. Asp. 534 (2017) 16–25, https://doi.org/10.1016/j.colsurfa.2017.04.055.

[40] S. Tcholakova, Z. Mitrinova, K. Golemanov, N.D. Denkov, M. Vethamuthu, K. P. Ananthapadmanabhan, Control of Ostwald ripening by using surfactants with high surface modulus, Langmuir 27 (2011) 14807–14819, https://doi.org/10.1021/la203952p.

[41] T.Y. Wei, K.L. Lim, Y.S. Tseng, S.L.I. Chan, A review on the characterization of hydrogen in hydrogen storage materials, Renew. *Sustain. Energy Rev.* 79 (2017) 1122–1133, https://doi.org/10.1016/j.rser.2017.05.132.

[42] M. Nishiyama, High-pressure microscopy for tracking dynamic properties of molecular machines, Biophys. Chem. 231 (2017) 71–78, https://doi.org/10.1016/j.bpc.2017.03.010.

[43] Q. Guo, J. Wang, C.B. Park, M. Ohshima, A microcellular foaming simulation system with a high pressure-drop rate, Ind. Eng. Chem. Res. 45 (2006) 6153–6161, https://doi.org/10.1021/ie060105w.

[44] L. Liebermann, Air bubbles in water, J. Appl. Phys. 28 (1957) 205, https://doi.org/10.1063/1.1722708.

[45] https://www.engineeringtoolbox.com/air-temperature-pressure-density-d_771.html last accessed on 2024.07.31..

[46] R. Sander, Compilation of Henry's law constants (version 5.0.0) for water as solvent, Atmos. Chem. Phys. 23 (2023) 10901–12440, https://doi.org/10.5194/acp-23-10901-2023.

[47] R. Battino, T.R. Rettich, T. Tominaga, The solubility of oxygen and ozone in liquids, J. Phys. Chem. Ref. Data 12 (1983) 163, https://doi.org/10.1063/1.555680.

[48] K. Drucker, E. Moles, Gaslöslichkeit in wässerigen Lösungen von Glycerin und Isobuttersäure, Z. F. üR. Phys. Chem. 75U (1) (1911) 405–436. Available from: https://www.degruyter.com/docu``ment/doi/10.1515/zpch-1911-7527/html.

[49] A. von Hammel, Gaslöslichkeit in wässerigen Lösungen von Glycerin und Chloralhydrat, Z. F. üR. Phys. Chem. 90U (1915) 121–125, https://doi.org/10.1515/zpch-1915-9007.

[50] Shin Etsu Silicone Fluid Technical Brochure, https://www.shinetsusilicone-global.com/catalog/pdf/kf96_e.pdf last accessed on 2024.07.31.

[51] P. Cannon, L.E. St. Pierre, A.A. Miller, Solubilities of hydrogen and oxygen in polydimethylsiloxanes, 236–236, J. Chem. Eng. Data. 5 (1960), https://doi.org/10.1021/je60006a027.

[52] I.G. Economou, Z.A. Makrodimitri, G.M. Kontogeorgis, A. Tihic, Solubility of gases and solvents in silicon polymers: molecular simulation and equation of state modeling, Mol. Simul. 33 (2007) 851–860, https://doi.org/10.1080/08927020701280688.

[53] M. Rosu, A. Schumpe, Influence of surfactants on gas absorption into aqueous suspensions of activated carbon, Chem. Eng. Sci. 62 (2007) 5458–5463, https://doi.org/10.1016/j.ces.2006.11.025.

[54] R.B. Bird, W.E. Stewart, E.N. Lightfoot. Transport Phenomena, second ed., John Wiley & Sons, New York, 2007.

[55] I.N. Tsimpanogiannis, O.A. Moultos, Is Stokes-Einstein relation valid for the description of intra-diffusivity of hydrogen and oxygen in liquid water? Fluid Ph. Equilibria 563 (2022) 113568 https://doi.org/10.1016/j.fluid.2022.113568.

[56] D. Chuan, F. Yurun, Measurement of diffusion coefficients of air in silicone oil and in hydraulic oil, Chin. J. Chem. Eng. 19 (2) (2011) 205–211, https://doi.org/10.1016/S1004-9541(11)60155-9.
[57] D.F. Evans, T. Tominaga, C. Chan, Diffusion of symmetrical and spherical solutes in protic, aprotic, and hydrocarbon solvents, J. Solut. Chem. 8 (1979) 461–478, https://doi.org/10.1007/BF00716005.
[58] D.F. Evans, T. Tominaga, H.T. Davis, Tracer diffusion in polyatomic liquids, J. Chem. Phys. 74 (1981) 1298–1305, https://doi.org/10.1063/1.441190.
[59] M. Liang, A. Kaintz, G.A. Baker, M. Maroncelli, Bimolecular electron transfer in ionic liquids: are reaction rates anomalously high? J. Phys. Chem. B. 116 (2012) 1370–1384, https://doi.org/10.1021/jp210892c.
[60] T. Yamaguchi, Coupling between translational diffusion of a solute and dynamics of the heterogeneous structure: higher alcohols and ionic liquids, J. Phys. Chem. B 126 (2022) 3125–3134, https://doi.org/10.1021/acs.jpcb.2c01053.
[61] C. Zhou, Y. Huang, Y. Zheng, Z. Hua, Hydrogen permeation behavior of rubber sealing materials for hydrogen infrastructure: recent advances and perspectives, Int. J. Hydrog. Energy 59 (2024) 742–754, https://doi.org/10.1016/j.ijhydene.2024.02.042.
[62] T.G. Poulsen, P. Moldrup, P. Schjønning, J.W. Massmann, J.Å. Hansen, Gas permeability and diffusivity in undisturbed soil: SVE implications, J. Environ. Eng. 124 (1998) 979–986, https://doi.org/10.1061/(ASCE)0733-9372(1998)124:10(979).
[63] A. Bondi, van der Waals Volumes and Radii, J. Phys. Chem. 68 (1964) 441–451, https://doi.org/10.1021/j100785a001.
[64] S. Kanehashi, T. Sato, S. Sato, K. Nagai, Microstructure and gas diffusivity of poly (dimethylsiloxane) sense membrane using molecular dynamics (MD) simulation, Trans. Mater. Res. Soc. Jpn. 37 (2012) 439–442, https://doi.org/10.14723/tmrsj.37.439.
[65] L. Tao, J. He, T. Arbaugh, J.R. McCutcheon, Y. Li, Machine learning prediction on the fractional free volume of polymer membranes, J. Memb. Sci. 665 (2023) 121131, https://doi.org/10.1016/j.memsci.2022.121131.
[66] B. Jönsson, H. Wennerström, P.G. Nilsson, P. Linse, Self-diffusion of small molecules in colloidal systems, Colloid Polym. Sci. 264 (1986) 77–88, https://doi.org/10.1007/BF01410310.
[67] M. Tokuyama, I. Oppenheim, On the theory of concentrated hard-sphere suspensions, Phys. A Stat. Mech. Appl. 216 (1995) 85–119, https://doi.org/10.1016/0378-4371(94)00280-7.
[68] A. Kasper, E. Bartsch, H. Sillescu, Self-diffusion in concentrated colloid suspensions studied by digital video microscopy of core−shell tracer particles, Langmuir 14 (1998) 5004–5010, https://doi.org/10.1021/la971089y.
[69] L. Ju, C.S. Ho, Oxygen diffusion coefficient and solubility in n -hexadecane, Biotechnol. Bioeng. 34 (1989) 1221–1224, https://doi.org/10.1002/bit.260340914.
[70] A. Gavezzotti, The calculation of molecular volumes and the use of volume analysis in the investigation of structured media and of solid-state organic reactivity, J. Am. Chem. Soc. 105 (1983) 5220–5225, https://doi.org/10.1021/ja00354a007.